energies

MDPI

Article

Wake width – discussion of several methods how to estimate it by using measured experimental data

Daniel Duda[1,*], Václav Uruba[1, 2] and Vitalii Yanovych[1, 2]

[1] Faculty of Mechanical Engineering, University of West Bohemia in Pilsen, Univerzitní 22, Pilsen, 306 14, Czech Republic;
dudad@kke.zcu.cz

[2] Institute of Thermomechanics, Czech Academy of Sciences, Dolejškova 5, Prague, 180 00, Czech Republic;
uruba@it.cas.cz

* Correspondence: dudad@kke.zcu.cz; Tel.:+420 377 638 146

Abstract: Several methods of defining and estimating the width of a turbulent wake are presented and tested on the experimental data obtained in the wake past an asymmetric prismatic airfoil NACA 64(3)-618, which is often used as tip profile of the wind turbines. Instantaneous velocities are measured by using the Particle Image Velocimetry (PIV) technique. All suggested methods of wake width estimation are based on the statistics of stream-wise velocity component. First, the expansion of boundary layer (BL) thickness is tested showing, that both, displacement BL thickness and momentum BL thickness do not represent the width of the wake. The equivalent of 99% BL thickness is used in the literature, but with different threshold value. It is shown, that lower threshold of 50 % gives more stable results. The ensemble average velocity profile is fitted by Gauss function and its σ-parameter is used as another definition of wake width. The profiles of stream-wise velocity standard deviation display a two-peak shape; the distance of those peaks serves as wake width for Norberg, another tested option is to include the widths of such peaks. Skewness (third statistical moment) of stream-wise velocity displays a pair of sharp peaks in the wake boundary, but their position is heavily affected by the statistical quality of the data. Flatness (fourth statistical moment) of the stream-wise velocity refers to the occurrence of rare events, therefore the distance, where turbulent events ejected from the wake become rare, can be considered as another definition of wake width. The repeatability of mentioned methods and their sensitivity to Reynolds number and model quality are discussed as well.

Keywords: Wake; Wake width; Particle Image Velocimetry; NACA 64-618; Skewness; Flatness;

Citation: Lastname, F.; Lastname, F.; Lastname, F. Title. *Energies* **2021**, *14*, x. https://doi.org/10.3390/xxxxx

Academic Editor: Firstname Lastname

Received: date
Accepted: date
Published: date

1. Introduction and motivation

Wake is a very important flow structure existing in many cases in the nature [Williamson1996]. Basically, it is produced in the area of fluid, which is slowed or stopped by the presence of an obstacle. The shear layers between the slowed and un-affected areas are turbulized and grows to both directions: (i) inside the wake turbulizing its interior and transporting surrounding momentum inside, which later leads to accelerating the flow there and to a "healing" of velocity deficit; and (ii) outside of the wake, which results into grow of the area affected by the obstacle and to its smoothing. Thus the wake is not structure with an easily-definable rigid boundary. Or it is?

Knowledge of the size of the area, where the flow is affected by some obstruction, has large importance in many engineering applications starting from design of wind farms [Wu2019, Abdulrahman2019] up to safety of transportation. For example, in our country, here is a political discussion about declaring minimal distance of overtaking on a road: especially in the case, when a motorized vehicle overtakes a bicycle. The risk of physical contact is only one half (and, of-course, the more dangerous one); the second

important issue is the question, when and where the wake past the large and fast-moving motorized vehicle reaches the bicycle with possible impact to its stability.

It is natural, that larger obstacles have larger wakes; it is less intuitive, that a faster flow produces slightly smaller wake. The latter is not a general rule, it depends on the turbulence regime, and the surroundings. Although the wake lacks some rigid boundary, the information about its width has to be quantified for comparative analysis of various cases and modifications.

A large amount of studies has been published concerning the wake past the circular cylinder [Williamson1996]. Circular cylinder is an easily accessible prototype of a general bluff body. An essential feature occurring at large range of Reynolds numbers is the stable configuration of alternating vortices discovered by Theodore von Kármán [Karman1911], which are responsible for periodic acoustic oscillations described by Vincenc[1] Strouhal in his famous work [Strouhal1878]. Although cylinder is prismatic (2D) shape, the wake turbulence displays three-dimensional characteristics [Williamson1987, Williamson2006] in dependence on regime. Several regimes [Roshko1955-Roshko1967] have been detected in that essential case in dependence on Reynolds number only, and many more, when the surface roughness, surrounding turbulence or angle of axis were taken into account.

The evolution of the wake is one of the key issues in aerodynamics. Because this phenomenon can characterize the various effects that occur when flow past an airfoil [Sadeghi, Davary, Liu]. It should be noted that the deficit of velocity is closely related to the drag force. Which can be derived solely from the velocity and pressure in a plane in the wake of the object [Terra2016].

In the most cases, PIV, hot-wire or pressure systems are used to estimate wake topology. The first two methods allow us to estimate not only the width and depth of the perturbation area, but also to investigate the structure of the turbulence flow. Classically characteristic wake dimensions are determined by the distribution of the average velocity behind airfoil [Hah, Kunze]. However, in some cases, they are estimated using the Reynolds stress components and degree of anisotropy of the flow. A comparative assessment of these analyses allows to clearly define the boundaries of the wake and to determine the transit zone around it [Solis]. This analysis is especially useful in the study of asymmetric profiles. Because in this case, the flow structure around the wake is more complex.

The present paper focus instead to the wake past an asymmetric airfoil NACA 64-618, which belongs to the family of "streamlined bodies", although, as will be shown, the real manufacturing procedures do not allow to reach this idealized state. We focus a single particular question: how thick (or wide) is the wake? We offer few definitions all based on statistics of stream-wise velocity, because this velocity component is easiest to measure by using multiple measuring methods like Particle Image Velocimetry, Hot Wire Anemometry or Fast-Response Aerodynamic Probe.

2. Materials and Methods

In this contribution, few methods for evaluation of wake width are compared. For this purpose, sample data are used; they are obtained by using commercial Particle Image Velocimetry [Tropea, Kopecký] system in an area past the asymmetric prismatic airfoil NACA 64(3)-618. The "slow" PIV is provided by Dantec company; it consists of 4 MPix camera Flow sense Mk II and solid-state double-pulse laser New Wave Solo of 500 mJ in single shot; the maximum repeating frequency of the system is 7.4 Hz. The field of view (FoV) is divided into gird of 64 × 64 interrogation areas, each covers area of 532 × 532 μm. The velocity vector detection is performed by using the Dantec Dynamic Studio software. The studied airfoil has been printed by using 3D printer Prusa Mk 2.5 and it was made of Polymerized Lactic Acid PLA [Inkinen2011]. More details about the observed flow in the wake at different Reynolds numbers and two angles of attack can be found in our publications [Duda2021b]. For comparison, the data at chord-based Reynolds number Re =

[1] [1] sometimes Vincent or Čeněk. The later form is a Czech home form derived from Italian home form Vincenzo (read "Vinčenc").

3.1·10⁴ are selected, the angle of attack $\alpha = 0°$. It has to be noted, that current experimental setup is not ideal due to quite high blockage ratio – the airfoil of chord equal to 80 mm and maximum thickness 14.5 mm is inserted into test section of width 125 mm (see the sketch in Figure 1).

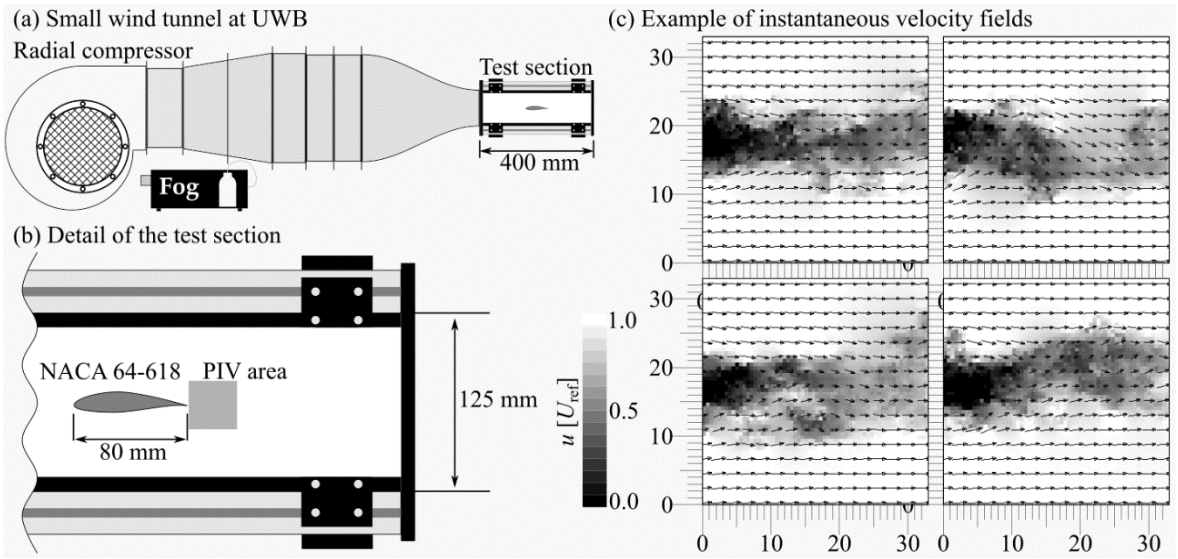

Figure 1. (**a**) Sketch of the "small" open wind tunnel used at the University of West Bohemia in Pilsen. The test section is 400 mm long, it has square cross-section of side 125 mm. (**b**) The localization of measured airfoil of chord 80 mm within the test section; its maximum thickness is 14.5 mm, thus the blockage ratio is 11.6 %. The area studied by PIV is just behind the trailing edge, it has dimension 33 × 33 mm, i.e. 0.4 × 0.4 chord length. The PIV plane is 45 mm from the bottom wall. (**c**) Example of few instantaneous velocity fields. The grayscale corresponds to stream-wise velocity component, U_{ref} means the reference velocity measured in empty wind tunnel, for presented data, it is equal to 11.5 m/s. Only every fourth velocity vector is shown. The entire ensemble of 1208 snapshots is animated in http://home.zcu.cz/~dudad/Ct300a00ab.gif (40 MB).

3. Discussion of wake widths

3.1. Expanding boundary layer approach

In contrast to wake studies, the set of boundary layer (BL) studies has unified standards for estimating the BL thickness. Again, BL is not a structure with some rigid boundary, the thickness is only an imaginary value, but its precise definition allows exact comparison and scientific exploration of questions about the effect of surface quality, surrounding turbulence intensity, pressure profile, etc. The main BL thicknesses are: the **99 % boundary layer thickness** δ_{99}, i.e. the distance, where the average velocity $\langle u \rangle(y)$ as the function of distance from the solid wall y reaches 99 % of the surrounding velocity u_r. This will be discussed soon. Now, let's mention the **displacement thickness** δ_1, which is based on the average velocity profile as well:

$$\delta_1 = \int_0^\infty 1 - \frac{\langle u \rangle(y)}{u_r} \mathrm{d}y \tag{1}$$

The integration goes from the solid surface (0) to infinity or, practically, "far enough". Its physical interpretation is, that it is the shift of an average streamline due to the presence of the solid surface [Bem2019, Duda2020].

The second main BL thickness definition is the **momentum thickness** δ_2

$$\delta_2 = \int_0^\infty \frac{\langle u \rangle(y)}{u_r} \left(1 - \frac{\langle u \rangle(y)}{u_r}\right) \mathrm{d}y \tag{2}$$

Its physical interpretation is, that δ_2 is the height of hypothetic area, whose momentum is missing from the flow, if the velocity profile was unaffected. The main ambiguity of these two definitions is the choice of u_r. For first look, it is clear. But, e.g. in the wind

tunnel experiments with incompressible fluid, the surrounding velocity is accelerated due to the presence of growing BL. Thus, one may ask what is better: the actual u_r in each position x, or some artificial constant independent on x? This question is much more actual in the case of wake past an obstacle – see the last isotach in Figure 2a, which demonstrates area with ensemble average velocity larger than the ongoing velocity U_{ref}, which is the first natural choice for u_r. However, the actual surrounding velocity may change with the distance (see Figure 3b). This is not only the issue of wind tunnel measurements; the in-field data can easily contain some velocity gradient as well. Figure 3a shows, that the choice of this parameter can influence the result significantly.

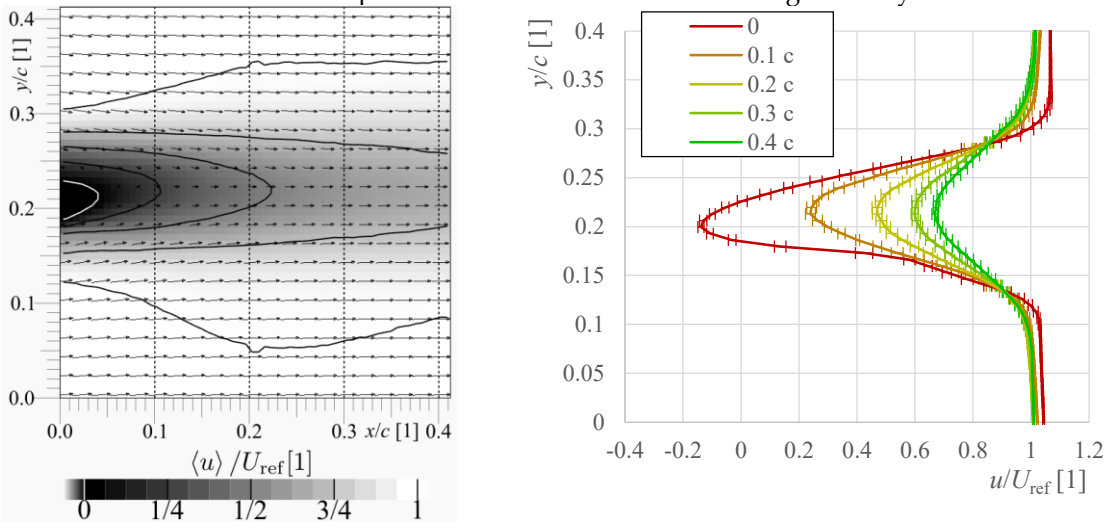

(**a**) (**b**)

Figure 2. Ensemble average stream-wise velocity. Panel (**a**) shows the map of average u (grayscale), the white isotach separates area of back flow, the last black isotach separates area of average velocity larger than reference velocity measured in empty wind tunnel. Panel (**b**) contains the velocity profiles at several distances from the trailing edge denoted as dashed lines in panel (a) distinguished via color: we apologize to readers with grayscale printer.

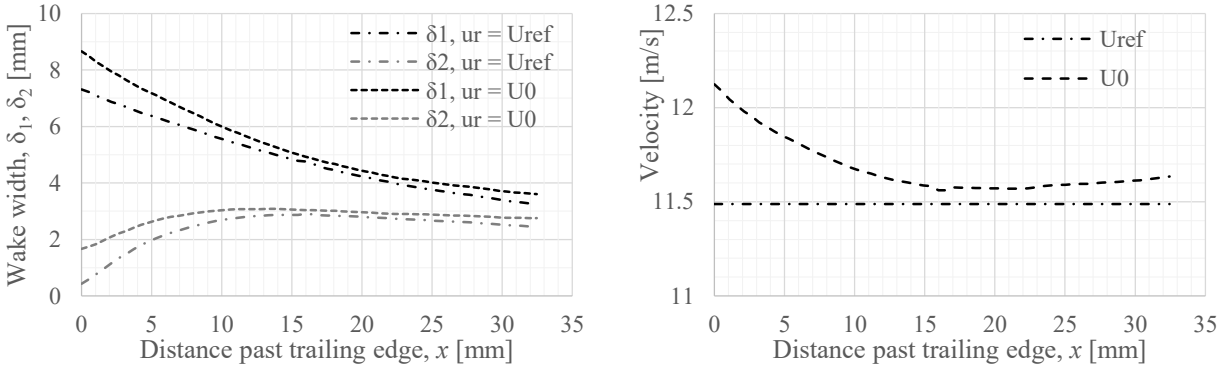

(**a**) (**b**)

Figure 3. (**a**) Wake width calculated according to the formulas for boundary layer thickness. The dash-dotted lines represent the calculation with constant $u_r = U_{\text{ref}}$, while the dashed line plays for usage of $u_r = U_0$, which is background of Gaussian fit and it develops with distance x. Dependence of these two velocities on x is displayed in panel (**b**).

The main "problem" with expanding the BL approach into the wake, is that the measured wake width *decreases* with stream-wise distance. It caused by the healing effect of the wake, when the centerline velocity deficit vanishes and thus the stream-line of average velocity field returns towards its unaffected trajectory. The momentum thickness δ_2 refers to the forces and drag coefficient rather to the width of the wake. But there has been

written a lot about the relation of velocity profiles to the drag coefficient, e.g. [Terra2016, Terra2017, Ragni2011, Gunasekaran2021] and many others.

To conclude, δ_1 and δ_2 surely offer an interesting measure of the wake, but its interpretation as wake width is misleading, because they do not describe the widening of the wake.

3.2. Threshold of average velocity

Natural and straight-forward method is to look, where the **velocity reaches threshold** θ:

$$\langle u \rangle \geq u_c = u_m + \theta \cdot (U_{\text{ref}} - u_m) \tag{3}$$

where u_m is the minimal velocity across the wake at some fixed stream-wise distance x. This approach with $\theta = 0.95$ is used by Barthelmie and coworkers in their study of wakes past offshore wind turbines [Barthelmie2006]. It is similar to the "99 % BL thickness" with the difference, that the threshold is related to the maximum velocity deficit, not to the absolute value of velocity. Here the problem with artificially chosen value of U_{ref} repeats as discussed above. Additional artificial parameter is the value of threshold θ – why one value should be better than another? Figure 4a shows, that the choice of 99 % is not ideal, as it is too close to the ambient flow and thus the results depends on variations of ambient velocity and uncertainties of measurement. One such issue is observable in Figure 4a as the bump in the middle of field of view, which correlates with similar bump in the spatial distribution of velocity (Figure 2a) and with drop of the fitted background velocity U_0 in Figure 3b; the reason is the connection of two camera chips at that location. But any study of flow *geometry* should be independent on such a small instrumental bug. The Barthelmie's choice of 95 % is more robust, but then one may ask, why not 90 % or 85 %? Let's try to set this threshold to 50 %. The threshold ½ is advantageous as the average velocity gradient is steep around that position and therefore the result is less dependent on the small perturbations in surrounding velocity and on the measurement uncertainty – in Figure 4a, the corresponding line is smoother. A last displayed option is $\theta = 0.394$, which is the drop of Gaussian function at distance of one σ from its center, $G(y = \sigma) = \exp\left(-\frac{\sigma^2}{2\sigma^2}\right) = \exp\left(-\frac{1}{2}\right) \approx 0.606$, which is the "distance" from background, distance from minimum is $1.0 - 0.606 = 0.394$.

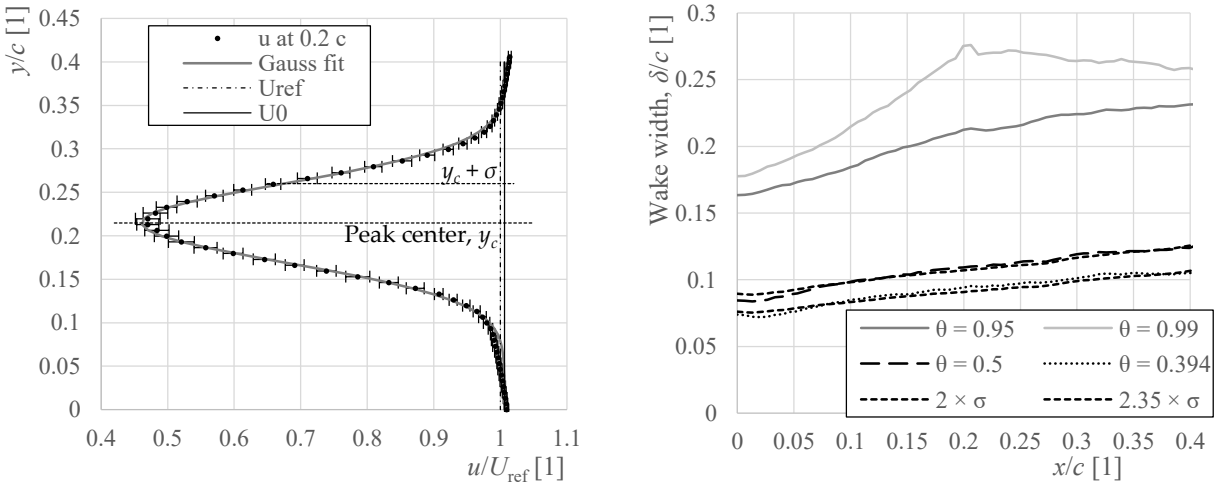

(**a**) (**b**)

Figure 4. Panel (**a**) shows data at one of velocity profiles (Figure 2b) with corresponding Gaussian fit. There is shown the constant value of U_{ref}, which is velocity measured in empty wind tunnel, and U_0, which is the background of Gaussian fit. (**b**) The comparison of mentioned methods based on threshold (first four) or on the Gaussian fit (last two).

3.3. Gaussian fit of average velocity profile

In fact, the threshold-based width wake depends only on few measuring points – the local minimum and then a pair of point of each side of the wake to determine the threshold position. Therefore, it is sensitive to some random rough measuring error in one point. The fitting procedure uses all measured points and thus single noisy point cannot destroy the result. On the other hand, fitting needs *a priori* knowledge of the velocity profile shape. The Gauss function occurs in many cases in nature as being product of the *Central limit theorem*, which is valid for *random processes*. But turbulence is not a random process, it just looks like random at the first look [Frisch].

Blondel et al. [Blondel2020] uses s*uper-Gaussian* with power slightly different from 2 to fit the velocity profile past a wind turbine rotor. It leads to better convergence, especially closer to the obstacle. But, too close to the obstacle, it does not work anyway, because the wake contains too strong "fingerprint" of the obstacle geometry. In the Blondel's case [Blondel2020], there is a sharper peak past the wind turbine hub surrounded by top-hut wake caused by the partly transparent wind turbine rotor. In our case, the velocity gradient is steeper past the pressure side (bottom in figures) than past the suction side – see Figure 2b, where the profile denoted "0" is evidently skewed towards the pressure (bottom) side.

The location of point, where the ensemble-average stream-wise velocity reaches one **σ of the Gauss function**, lies pretty inside the wake, therefore it might to be multiplied by certain constant in order to shift it systematically towards the real wake boundary. When one wants to mimic the value, where the velocity drop reaches half of the centerline drop, then he has to multiply σ by $\sqrt{-2\ln\frac{1}{2}} \approx 1.177$, to get the distance of those points multiplied twice, the multiplicator is 2.3548. By this way, any desired level (e.g. 95 % or 99 %) can be reached without being affected by uncertainty in surrounding velocity or some noise on the velocity profile. Still, it is just multiplication by constant, therefore this step can be skipped for comparative studies, as it is done e.g. by I. Eames, C. Jonsson and P.B. Johnson [Eames2011] in their study of growth of wake past circular cylinder.

3.4. Statistics of instantaneous wakes

All the other described methods are based on averaged wake structure. However, that average wake is far different from the instantaneous picture, which shows not only widening of the wake, but its meandering as well. Detection of the wake on instantaneous snapshots is possible by fitting the transverse profile of the instantaneous stream-wise velocity by using the Gaussian function. These fits converge less than that of the average velocity profile, because the profile shape is quite wild (see Figure 5b), but still, the wake centerline and width can be extracted. Figure 5a shows the found position of wake center and wake width on a single snapshot.

The ensemble average and standard deviation of the found wake widths for each stream-wise position past the trailing edge are displayed in Figure 5a. Close past the trailing edge, the average of instantaneous wake widths corresponds to the width of average wake, while it shows larger discrepancy in later stages. This issue reveals an important fact, that the actual wake is smaller than visible in the averaged data, because part of its width is caused by meandering of its position. The meandering of the wake affects the standard deviation of the wake center position, which is displayed in Figure 5b in term of error bars. The difference between average of instantaneous wake widths and width of average wake at end of the field of view, $x/c = 0.4$, is $0.017 \cdot c$, the standard deviation of the wake position at same location is $0.026 \cdot c$.

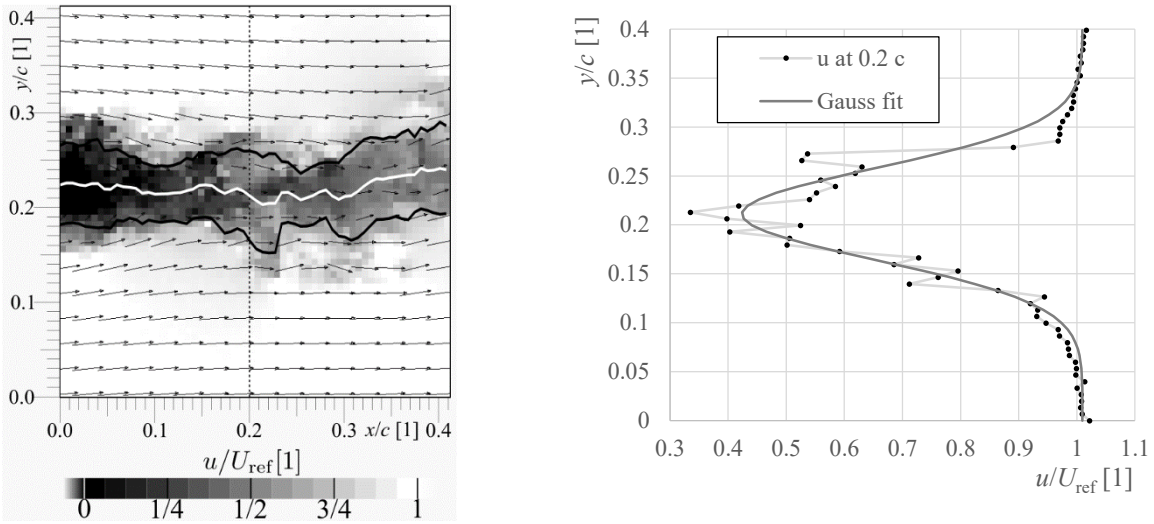

(**a**) (**b**)

Figure 5. Instantaneous stream-wise velocity. Panel (**a**) shows the map of u (grayscale) normalized by reference velocity. The white line represents the centers of Gaussian fits in transverse profiles, the pair of black lines are the centers plus/minus the σ-parameter of the fit. Panel (**b**) shows a single particular Gaussian fit at the stream-wise distance denoted as dashed line in panel (a).

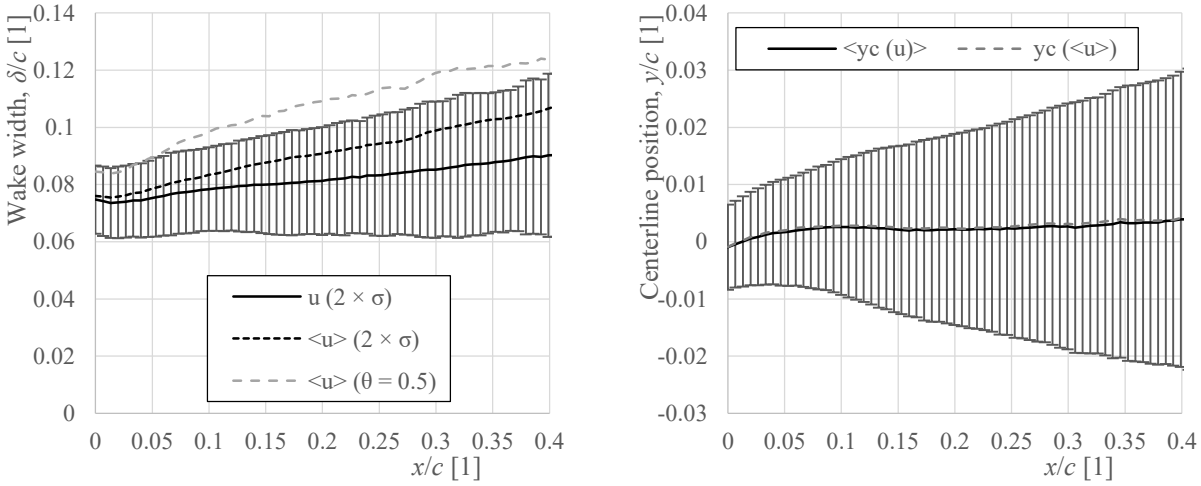

(**a**) (**b**)

Figure 6. Panel (**a**) compares the wake width calculated as average of the instantaneous wake widths (Figure 5) with the wake width of ensemble-averaged stream-wise velocity by using the Gauss fit (black short-dashed line) and by using the threshold method (gray dashed line). The error bars represent the standard deviation of the instantaneous wake widths in each position. Panel (**b**) shows the position of wake centerline calculated on instantaneous (black solid line) or ensemble-averaged (gray dashed line) velocity field. Error bars are the standard deviation of the instantaneous wake positions.

3.5. Standard deviation of stream-wise velocity

An important aspect of turbulent wake is the increase of turbulence inside it. The turbulence can be easily quantified by using the standard deviations of the measured velocity components:

$$\sigma[u] = \sqrt{\langle (u - \langle u \rangle)^2 \rangle} \quad (4)$$

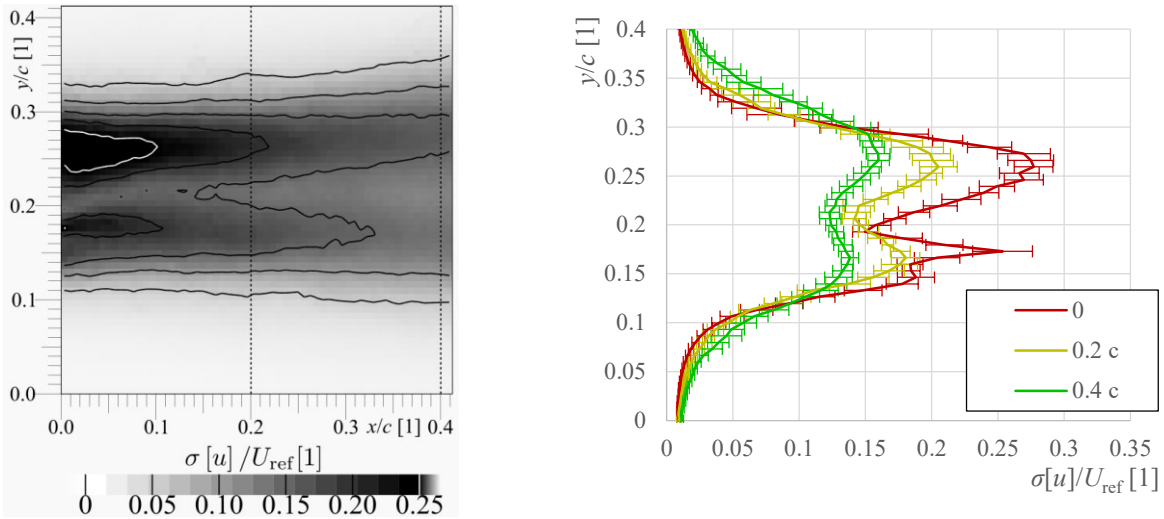

(**a**) (**b**)

Figure 7. Standard deviation of stream-wise velocity. Panel (**a**) shows the map of $\sigma(u)$ (grayscale) normalized by reference velocity. Panel (**b**) contains the standard deviation profiles at several distances from the trailing edge denoted as dashed lines in panel (a); we apologize to readers with grayscale printer.

In the wake past a streamed body (which is the case of airfoils under non-stall conditions), the fluctuation wake pattern is dominated by double maxima of the stream-wise component, which form past the boundary layers. In the case of asymmetric body, these maxima are asymmetric as can be seen in Figure 7 – the bottom maximum past pressure side is smaller than the top one past the suction side, due to the development of boundary layer under different pressure gradients. Near the wake axis, the fluctuations in transverse direction dominate, which is caused by the separation at the trailing edge and the alternating dominance of one or the other boundary layer. In the wake past a bluff body, this effect would be dominating over the entire wake. A second reason, why we want to explore the standard deviation of stream-wise direction rather than Turbulent kinetic energy or the standard deviation of transverse velocity component, is that this velocity component is easily obtainable by other methods e.g. by single-wire hot wire anemometry (HWA) or by fast response pressure probes (FRAP).

Norberg [Norberg1986] investigated the flow around circular cylinder. Among others, he looked for the point of minimal wake width, because, at that position, the vortices are fully formed and start their diffusive convection downstream (he states). As a side product, he suggests definition of wake width as the **distance of maxima** of stream-wise velocity fluctuations. This definition is used e.g. in [Cao2018,] Application of this approach to our data is displayed in Figure 8b as solid line. A strong "leveling" is caused by the finite resolution of our PIV grid. To avoid discretization of the maxima positions, the fitting procedure can be used again, now with the double-Gauss function:

$$G_2(y) = A_t \exp\left\{-\frac{(y-y_t)^2}{2\sigma_t^2}\right\} + A_B \exp\left\{-\frac{(y-y_b)^2}{2\sigma_b^2}\right\} + B \quad (5)$$

where B is the background, A_T and A_B are the amplitudes of top and bottom peak respectively, y_t and y_b are the peak positions and σ_t and σ_b are the corresponding peak thicknesses. Again, *a priori* expectation of the profile functional dependence is needed, whose validity is limited – see the poor convergence in the bottom part of the profile in Figure 8a. On the other hand, the quite high number of fitting parameters is able to fit almost everything and thus the physical interpretation of convergence can be easily misleading. The **distance of double-Gauss peaks** is displayed as dashed line in Figure 8b. This value is systematically larger than Norberg's approach, but the development with distance is

clearly smoother as all profile points are used instead of single maximum only, which can be easily shifted by some local noise.

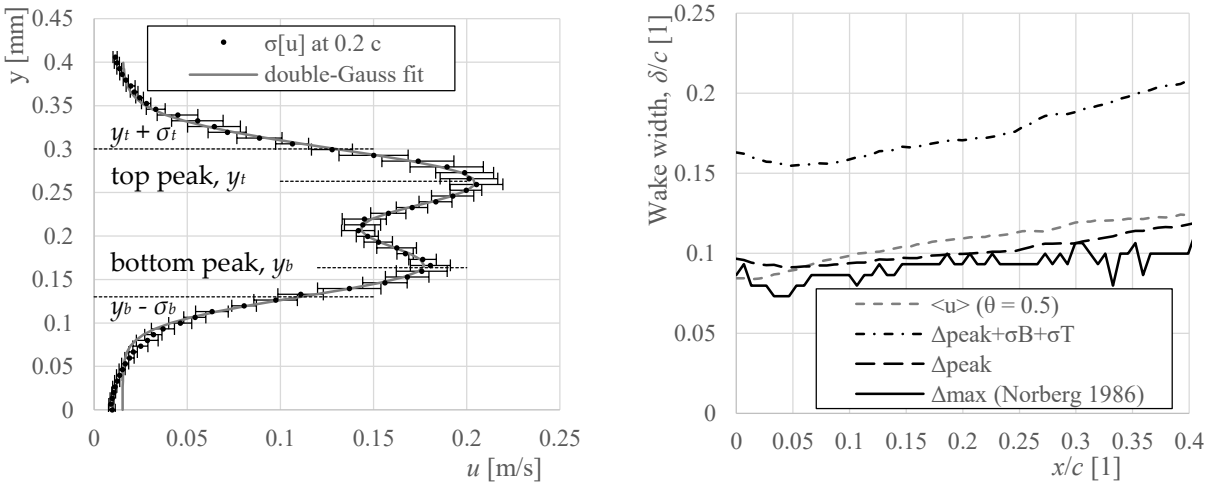

(**a**) (**b**)

Figure 8. Standard deviation of stream-wise velocity. Panel (**a**) shows the map of $\sigma(u)$ (grayscale) normalized by reference velocity. Panel (**b**) contains the standard deviation profiles at several distances from the trailing edge denoted as dashed lines in panel (a).

The distance of peaks does not contain the splashing of the fluctuation structures. In order to adhere it, we combine this **distance of double-Gauss peaks plus widths of peaks**. In respect to the average velocity profiles, the later method is able to distinguish the reduction of wake width in the near wake (at around $x/c = 0.05$ in Figure 8b), because the double-Gauss function is more robust to the non-ideal shapes of profiles caused by the "fingerprint" of obstacle geometry.

The first and second statistical moments displayed up to here show a smooth vanishing with increasing distance from the wake axis. Therefore, the wake width cannot point to some exact boundary of the wake, it can only show, where it is weak enough. Any one of these methods (when used systematically) can tell us, how wake width develops with distance or with Reynolds number, or if some shape modifications increase or decrease wake width; and it is capable to answer many more interesting questions. But, is it possible to point to some distance and tell: "the wake ends here! "? We are confirmed than yes.

3.6. Flatness – the fourth statistical moment

The fourth statistical moment is called *Flatness*, sometimes (e.g. in Wikipedia) *Kurtosis*. It is defined as

$$F[u] = \frac{\langle (u - \langle u \rangle)^4 \rangle}{\sigma^4[u]} \tag{6}$$

It is normalized by standard deviation $\sigma[u]$; therefore, it is dimensionless. It is possible to proof, that $F[x]$ of some Gaussian-distributed random quantity x is equal to 3, which is then a reference value.

The physical interpretation of this statistical quantity is, that it refers to *strong rare events* (in popular statistics, they are called "black swan"); in turbulence, they rely to *intermittency* [Frish], which shows that turbulence is not a set of random events, but a set of coherent structures – vortices. This is much stronger in *quantum turbulence* [Skrbek2021], where the vortices are quantized, all having same circulation, they do not overlap and therefore, if the turbulence intensity is weak, there is only less number of still same strong vortices instead of weaker vortices in classical turbulence. The consequence is, that the velocity probability distribution deflects from Gaussian distribution to a polynomial distribution [LaMantia2013] with exponent -3, whose flatness converges to infinity instead

of 3 as it does for Gaussian distribution [LaMantia2016]. But at larger scales, the quantum turbulence mimics the classical one including the higher-order effects such as steady streaming [Duda2017].

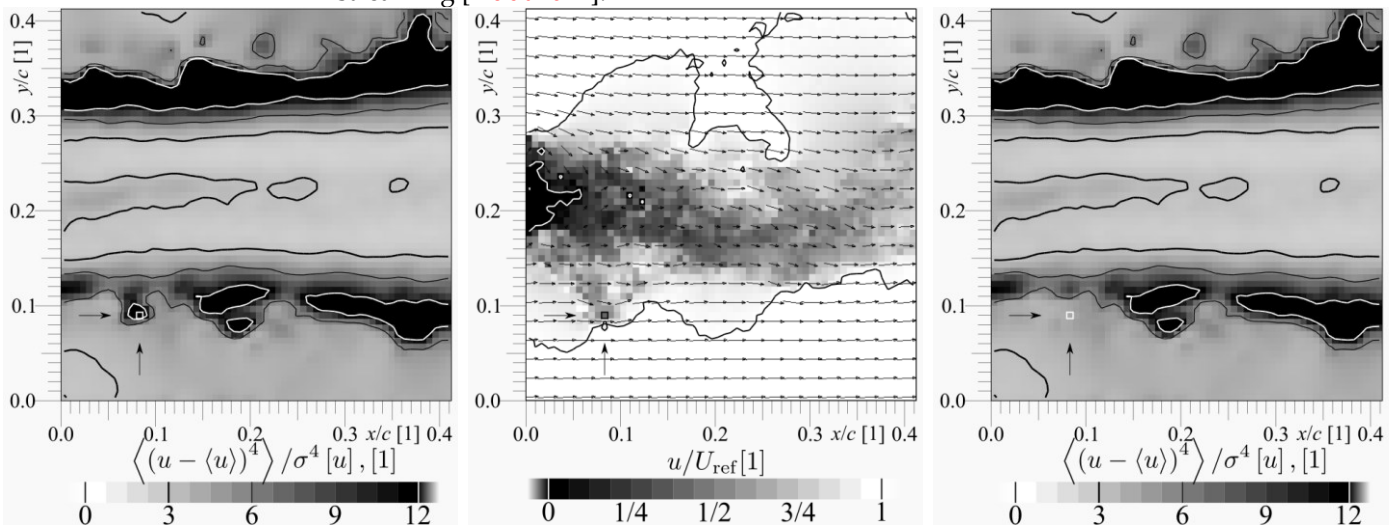

Figure 9. (**a**) Spatial distribution of stream-wise velocity flatness; the thick isoline refers to value of 3, the thin black isoline to 6, the white isoline to values greater than 12. (**b**) The instantaneous velocity field with value most different from the average in the point denoted by rectangle and a pair of arrows in bottom left corner. Note, that this snapshot is a regular case, it is not noisier than the others, only there is some fluid of lower velocity ejected from the wake into the surroundings hitting the denoted point. (**c**) Spatial distribution of flatness of the ensemble without the snapshot (b). Note that removal of single case of 1208 significantly decreases the flatness signal in the denoted point.

In the case of wake turbulence, the high flatness signal tells us, that there is flow with some turbulence intensity, which is time-to-time visited by some structure stronger than it would correspond to the usual statistical distribution. This will be demonstrated on a single case. Figure 9a shows the spatial map of flatness of stream-wise velocity component; note, for example, the local peak in the left bottom corner denoted by white rectangle and black arrows. Figure 9b shows the snapshot, which differs most from the ensemble average at the denoted point. It is a regular snapshot with no more noise than the others, only here is some turbulent structure, which ejects the low-momentum fluid from the wake into the faster surroundings. This is not against the rules, but it is a rare event. This event produces high flatness signal, which is proven in Figure 9c showing the flatness of all other snapshots. Consequently, the signal around the denoted point refers to regular fluctuations, thus flatness is slightly larger than 3.

This behavior of flatness inspired us to define the wake boundary as the line, over which the fluctuations become rare, i.e. **flatness grows over 6** (twice the Gauss reference vale). The grow of flatness is quite steep and it grows to large values, see Figure 10a. The main disadvantage is, that it needs high statistical quality of the ensemble –there is over 1200 snapshots, which is not small amount, and the flatness map is still irregular, especially, at the outer boundary. Only a one single snapshot with wrong data can easily disturb flatness value. The uncertainty of flatness is really high in the case of PIV data (see error bars in Figure 10a), however, the flatness increase is steep enough to give a reasonable wake boundary localization despite the large uncertainty.

The average velocity itself could lead easily to misleading conclusions. For example, imagine an observer staying somewhere next to the wake. When taking into account the average velocity and turbulence intensity only, one would expect, that the observer observes velocity slightly smaller than the surrounding one with turbulence intensity slightly larger. But in fact, he observes the surrounding velocity and turbulence intensity

most of the time, with few blows of the wake fluid. This is an important difference especially for the problem of mechanical stability or turbulent mixing.

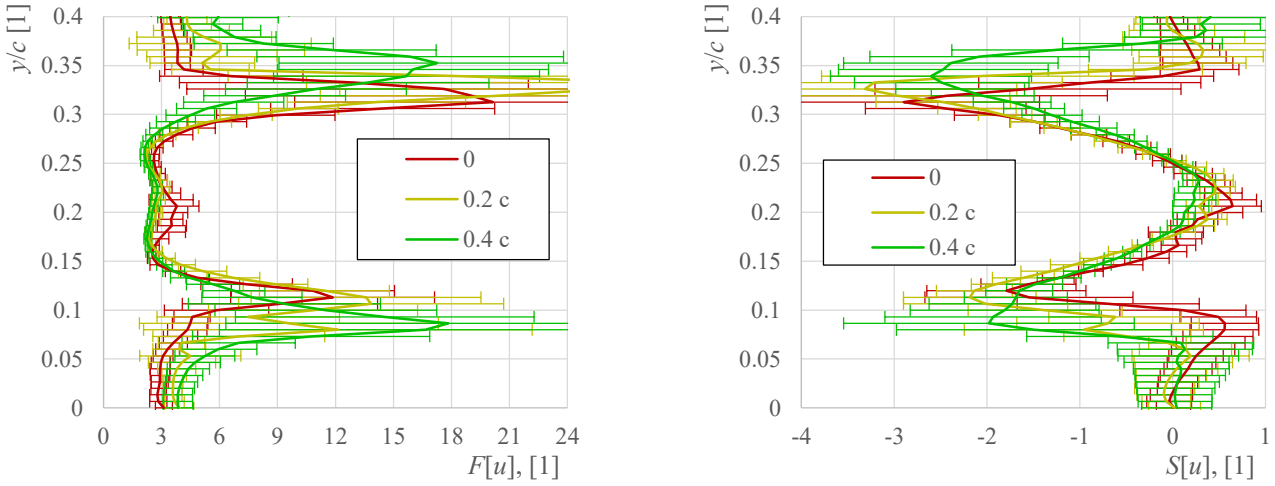

(**a**) (**b**)

Figure 10. (**a**) Profiles of flatness coefficient of the stream-wise velocity component. (**b**) Profiles of the skewness of stream-wise velocity component at depicted distance past the trailing edge distinguished via colors: we apologize to readers with grayscale printer.

3.7. Skewness – the third statistical moment

The asymmetry in velocity distribution can be quantified in terms of the skewness, sometimes called coefficient of asymmetry, defined as the third central statistical moment:

$$S[u] = \frac{\langle (u - \langle u \rangle)^3 \rangle}{\sigma^3[u]} \tag{7}$$

At the boundary of the turbulent wake, the average velocity is smaller than in the surroundings, which is caused by the mixing with wake fluid. When the shear layer is visited by the slower fluid from central region, then this visit decreases the velocity here more probably than increases. This asymmetry produces negative skewness signal at the wake boundary. On the other hand, in the central region, the visit from outside increases the velocity, thus the skewness is slightly positive there.

Figure 11a shows the spatial distribution of stream-wise velocity skewness across the field of view with four depicted regions. Figure 9b displays the probability density of instantaneous variations of u in those regions. The central region is almost symmetric, however, note that the maximum occurrence (peak in the solid line in Figure 11b) is shifted in respect to the average (zero in the horizontal axis in the plot). The inner part of the shear layer (dashed line denoted SL1) displays more of slower events than faster events; in the outer shear layer region (SL2, dash-dotted line) contains two merged peaks and the surrounding region displays distribution more similar to the Gaussian, note that it is much sharper in absolute values, see the inset of Figure 11b.

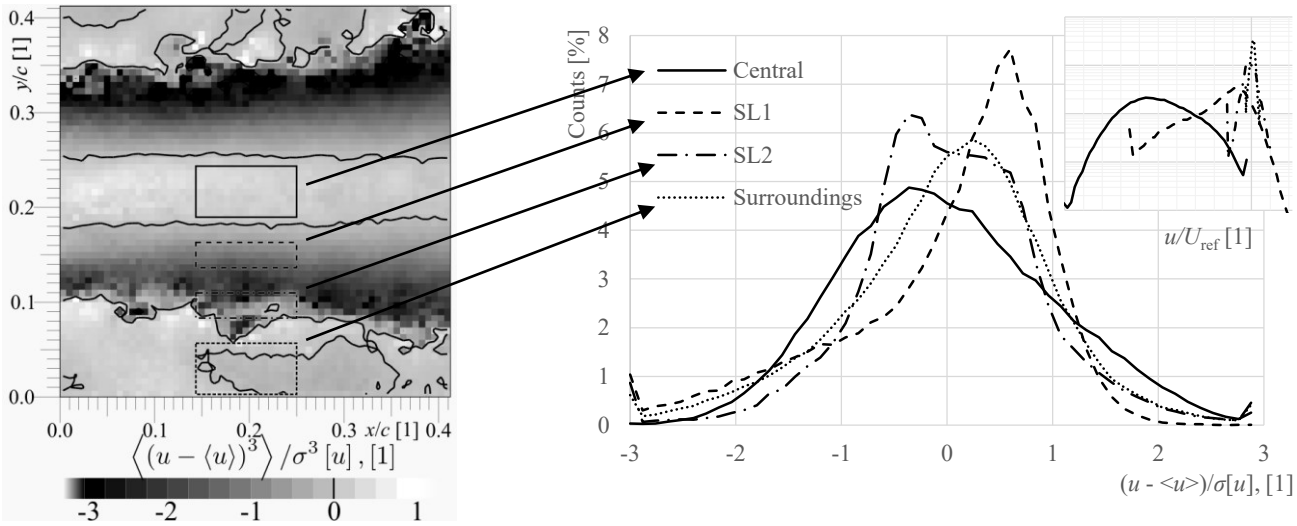

(**a**) (**b**)

Figure 11. (**a**) spatial map of the skewness of stream-wise velocity component. (**b**) Probability density function (PDF) of the instantaneous stream-wise velocities within the four denoted rectangles, solid line in the wake central region, dashed line in the inner shear layer (SL), dash-dotted line in the outer shear layer and the short dashed line in the surrounding region. The *u* values are normalized by the local average and standard deviation. The inset shows the PDF as the function of velocity and it shows different widths and positions of the distributions (note the logarithmic scale in inset).

It has been reported by A. Mariotti and G. Buresti [Mariotti2013], that skewness of stream-wise velocity past a bullet-like body (head is rotating ellipsoid of 3 : 1 axis ratio; body is a cylinder with sharp base) contains negative peak in the transverse profile and that the position of this peak corresponds to the downstream projection of the obstacle surface. Their work inspired us to define the wake width as the **distance of pair of negative peaks in stream-wise velocity skewness**. The skewness transverse profiles past NACA 64-618 airfoil are displayed in Figure 10b. Note, that the wake past a bluff body may not contain such sharp peaks. The pattern of skewness is similar to that of flatness. It is not a random coincidence – both statistical moments reflect the same phenomenon of mixing the fluids from wake center and from surroundings.

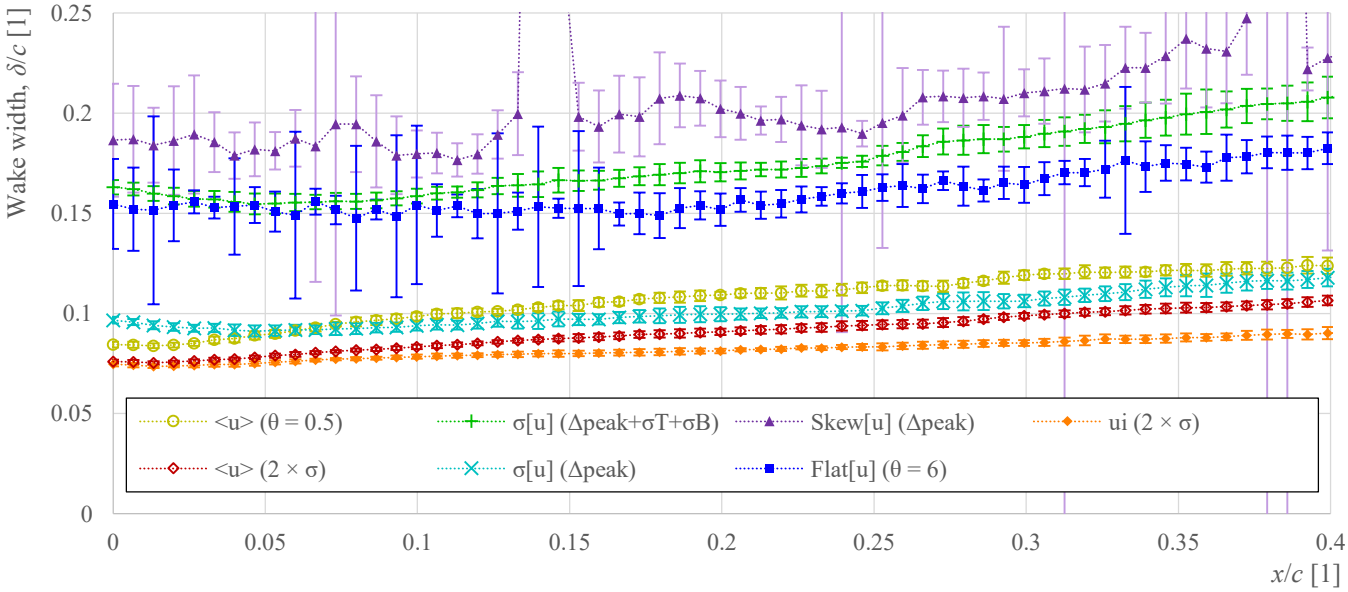

Figure 12. Comparison of the discussed definitions of wake width past the airfoil NACA 64-618 at zero angle of attack. Horizontal axis is the distance past trailing edge; all lengths are normalized by the airfoil chord. Golden circles: the distance of points, where average velocity deficit crosses half (threshold $\theta = 0.5$) the maximum velocity deficit. Maroon diamonds: twice the thickness σ of the Gauss function fitted to the average velocity profile. Orange diamonds: the average of

wake widths fitted to each snapshot. Cyan Xs: the distance of double-Gauss peaks fitted to the profile of standard deviation of stream-wise velocity. Green crosses: distance of mentioned peaks plus the thicknesses of those peaks in the profile of standard deviation of stream-wise velocity. Violet triangles: distance of double-Gauss peaks fitted to the profile of stream-wise velocity skewness (third statistical moment). Blue rectangles: distance of points, where the stream-wise velocity flatness reaches the threshold $\theta = 6$, i.e. 2×3, the Gauss reference value.

Figure 12 shows the wake width determined via double-Gauss fitting of skewness (triangles) and via thresholding of flatness (squares). The (ir)regularity of their development reveals that the usage of all profile points during fitting procedure does not need to be advantageous in all cases: the poorer statistical convergence at the outer wake boundary is inherited within the position of skewness peaks, while the threshold at inner part of the wake boundary is more stable. Unfortunately, some meaningful threshold value for the skewness profile is unknown at this moment. In the case of Hot Wire Anemometry (HWA) or Laser Doppler Anemometry (LDA) the statistical quality is not a problem, because those methods are capable to gain millions of data points at each location, while PIV method used here is limited to maximum thousands of snapshots.

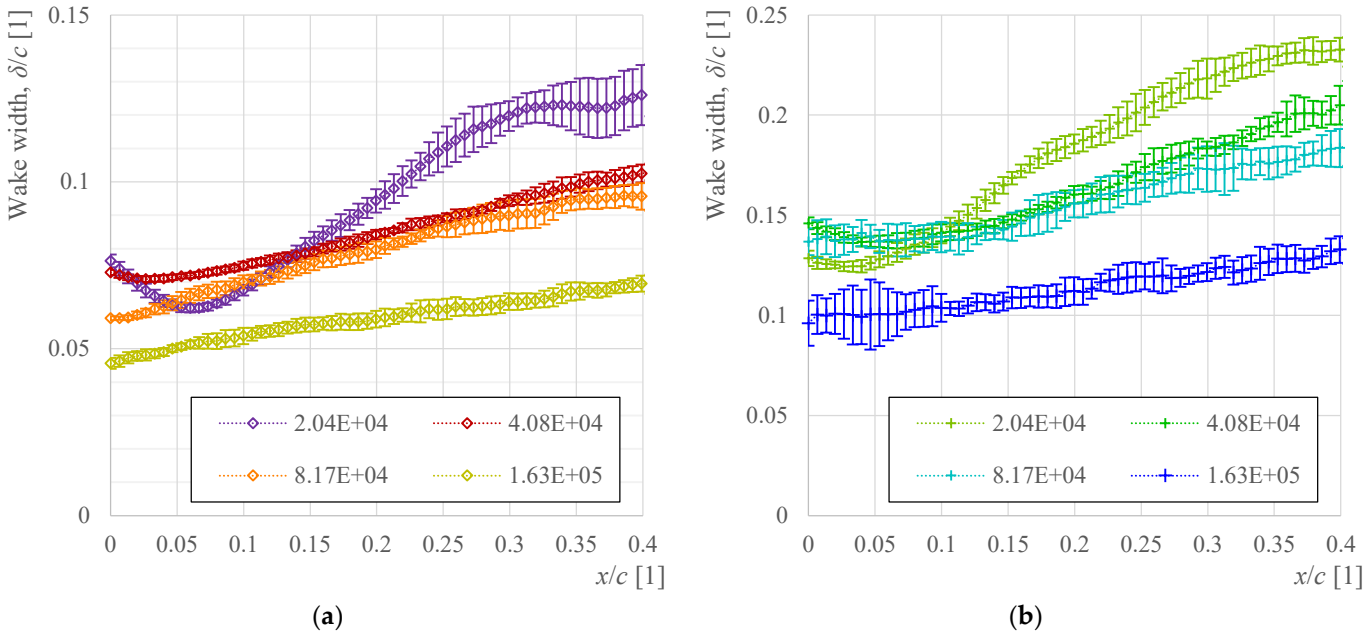

Figure 13. Wake widths past airfoil at different Reynolds numbers. Panel (a) shows the wake width calculated as the σ-parameter of Gaussian fit of the ensemble-averaged stream-wise velocity. Panel (b) shows the wake widths calculated by using standard deviation of stream-wise velocity fitted by double-Gauss function, the peak distance plus the width of bottom σ_B and top σ_T peak. Note the Re explored up to here is $6.1 \cdot 10^4$, it is not plotted here.

4. The effect of Reynolds number

Exploring the wake widths at different Reynolds numbers reveals one important detail: the described methods based on higher statistical moments may not work under laminar conditions. It is not surprise, because the laminar flow does not contain fluctuations. The only source of fluctuation is the random time of snapshots (the acquisition system not synchronized with the vortex shedding in laminar wake). The average of instantaneous wake width shows the same values as the Gaussian-fitted value on average velocity field in the laminar regime at Reynolds numbers 1.6 and $2.0 \cdot 10^4$, while the meandering of the centerline expressed as the standard deviation of its ensemble-averaged positions reaches maximal values at lowest Re (see Figure 14b, circles). The laminar wake is a different pattern than the turbulent wake, therefore different methods shall be applied for its exploration.

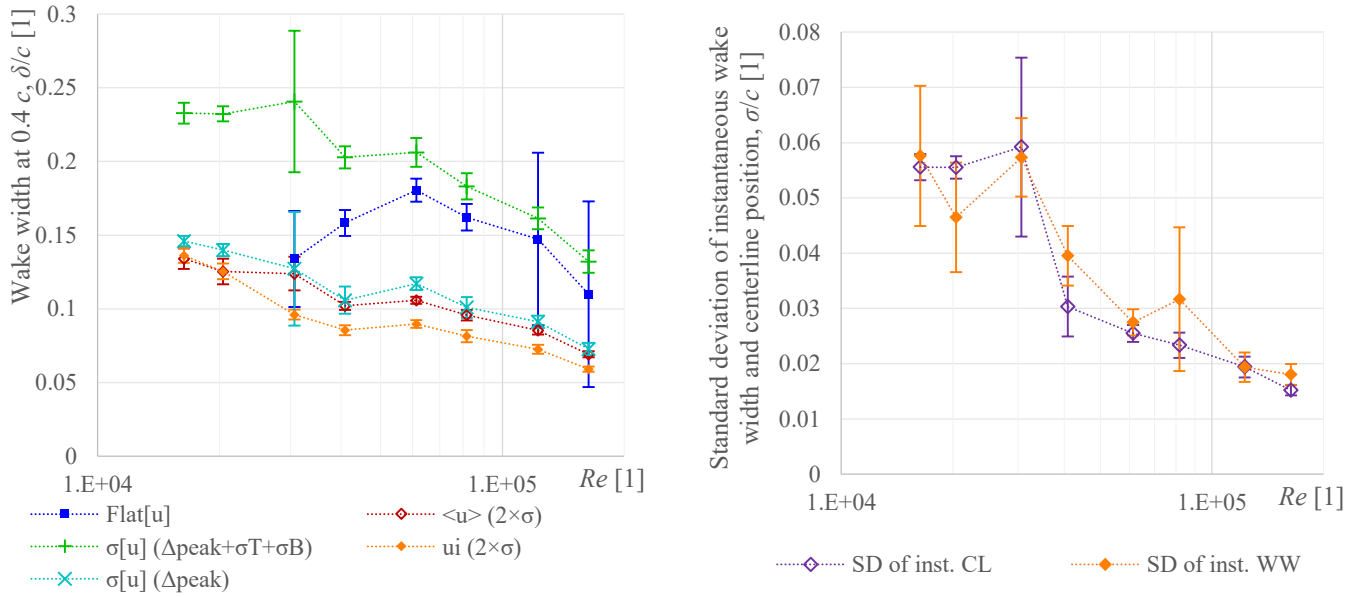

(**a**) (**b**)

Figure 14. (**a**) Comparison of possible wake width definitions at distance x/c = 0.4 past the airfoil NACA 64-618 trailing edge as a function of chord-based Reynolds number. Empty maroon diamonds denote the Gaussian fitting of average velocity profile, filled orange diamond the Gauss fitting of instantaneous velocity fields, the green crosses represent wake width based on peaks of stream-wise velocity standard deviation, cyan Xs represent the fluctuation peak distance only, and the blue squares represent the threshold of stream-wise velocity flatness, which fails for laminar flow, therefore, it is not plotted there. (**b**) Standard deviation of the instantaneous wake width calculated by using Gaussian fit (orange filled diamonds) and the standard deviation of the wake centerline position (violet empty diamonds), which can be interpreted as wake meandering.

Figure 14 shows the wake width determined by discussed methods at fixed position past the obstacle, but this plot does not contain the information about the wake development with distance past the obstacle. Eames et al. [Eames2011] derived, that the functional dependence of wake width follows the square root of the distance past obstacle, because, as the turbulence intensity decreases due to splashing, there is less energy to eject turbulized fluid out. However, this effect takes place in developed wake, while the example used here covers only the near wake region, where the development of wake width with distance roughly follows a simpler linear function (see Figure 12 and 13) since the position x/c = 0.1:

$$\delta_w(x) = a \cdot (x + x_0) \tag{8}$$

where a is the wake grow rate (Figure 15b) and x_0 can be understand as a virtual origin of the wake upstream the obstacle trailing edge (Figure 15a). Imagine, that the wake widths discussed here differed only by a scale, then the parameter a differed as well, but the parameter x_0 might reach same values. Figure 15a shows that it is the case at lower Reynolds numbers in laminar regime, while at higher Re, x_0 differs among methods. The methods based on average velocity display origin closer to the trailing edge, while the methods employing fluctuations virtually originate farer upstream. All points display grow with Reynolds number (i.e. originating farer upstream), with increase in the range of transient flow from laminar to turbulent regimes. The linear wake grow rate systematically decreases with Reynolds number, except for the transient area, therefore one can expect, that this airfoil produces smaller total wake area including the unobserved downstream development at higher Reynolds numbers, which physically supports the observation of Du et al. [Du2016] that this airfoil has a good performance at higher Re. The wake width,

which is affected less in the transition regime, seems to be the wake width based on stream-wise fluctuations, this width displays the largest grow *a*.

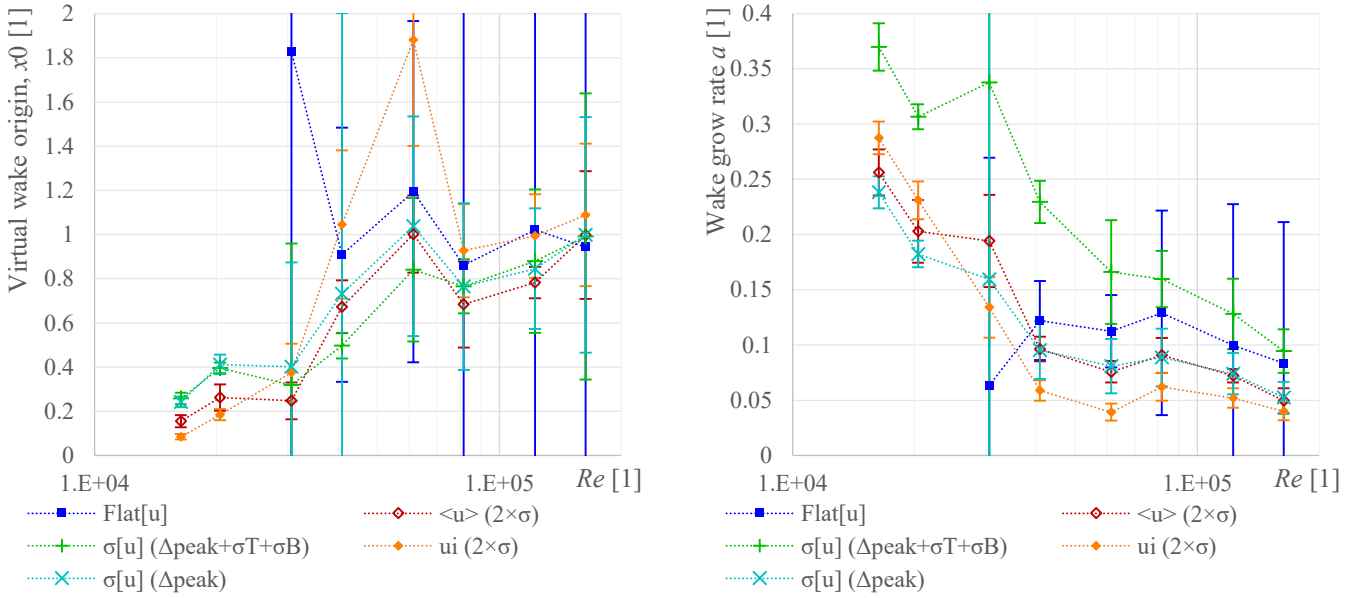

(**a**) (**b**)

Figure 15. (**a**) Virtual origin x_0 of the wake width, if its stream-wise development is approximated by linear function (8). The uncertainty of flatness-based wake width is so high, that it is not plotted. (**b**) the grow rate *a* of the wake as a function of Reynolds number. The symbols are the same as in Figure 14.

5 Uncertainty

The uncertainty of such a complex method, as PIV is, consists of many error sources [Sciacchitano2019, Sciacchitano2016] starting from the image preprocessing, through cross-correlation peak detection up to statistical issues. Generally, the measurement uncertainty projects into two main effects: the systematic error and the statistical noise. The systematic error in velocity does not affects the wake width, which is a geometrical property, but it is affected by the uncertainty in calibration (which affects the measured velocity as well) and in boundary conditions (input velocity, geometry of the tunnel and obstacle). It is difficult to beat the systematic error without applying some other method, which would have its own sources of uncertainty. On the other hand, the statistical noise is naturally present in any measured series and its level might decrease with number of samples as $\sim N^{-1/2}$ [Sciacchitano2016]. Its effect is illustrated in Figure 16 showing the wake widths obtained by several discussed approaches as a function of number of snapshots taken into account. At smaller number of snapshots, all methods give untrustworthy results; the fitting methods stabilize after approx. 100 points, the threshold of average velocity definitely needs more, while the methods based on higher moment do not seem to stabilize at all. This empirical approach is used to *estimate* all the uncertainties presented in this work: the ensemble is virtually separated into 10 subsets, the analysis is performed on each of them and the standard deviation of the set of results is used as the estimation of unknown uncertainty.

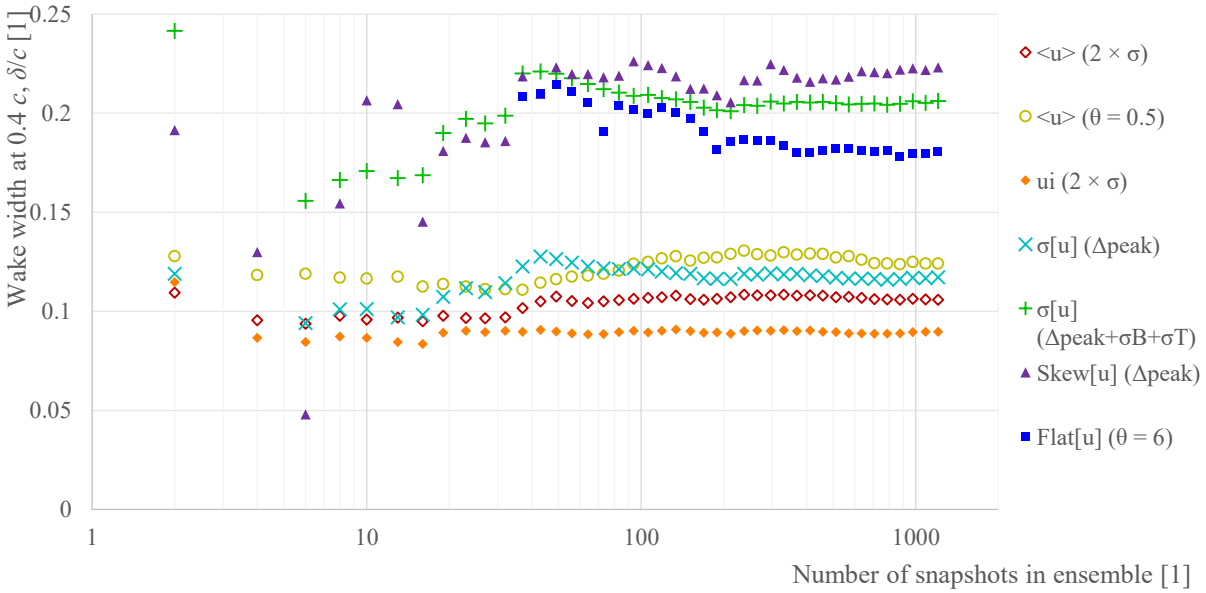

Figure 16. Wake widths at constant distance $x/c = 0.4$ as a function of number of snapshots used for averaging.

6 Conclusion

The present article compares several methods of calculating wake width. All mentioned methods are based on a transverse profile of the stream-wise velocity component, because this component is accessible by most measuring techniques. Basically, the wake width can be found from points, where the profile of some quantity reaches a chosen threshold, or as a result of fitting procedure, where some functional profile shape has to be known. The advantages and disadvantages are listed in Table 1. Table 2. compares the statistical momenta of stream-wise velocity component, which can show the wake boundary. As it is often in such cases, the property, which is advantageous for one application, can be disadvantageous for another and vice versa.

Table 1. The possible mathematical methods of extracting parameters of some data profile.

Method	Advantages	Disadvantages
Threshold	- Simple and robust. - Easy to implement. - The physical interpretation is straight forward.	- Results depends on a single point or its surrounding, therefore more sensitive to noise. - Threshold choice need some justification. - The thresholded point has to be visible (inside field of view or traverser range).
Fitting	- Result depends on all data points of the profile. - Not need to see the entire profile. - More stable on noisy data.	- Need for an a priori knowledge of the functional dependence of the profile. - Danger of fake local optima, especially in the cases of too many fitting parameters, or when the real functional dependence does not follow the expected one.

Table 2. The momenta of stream-wise velocity, which have been examined in this contribution.

Moment of u	Advantages	Disadvantages
Average	- Easiest to obtain by most measuring and computational techniques. - A simple functional profile in later stages, therefore only a part of the wake has to be measured. - Good repeatability	- The average velocity does not draw the wake sharply - The resulting width is a product of convention rather than of some physical effect.
Standard deviation	- Refers to fluctuations, which is the key feature of any flow structure. - Reasonable (but not excellent) repeatability.	- It is not yet clear, how and when the double-peak character disappears.
Skewness	- Refers to the entrainment effect of the turbulent flow.	- Need for high statistical quality - The outer edge of the wake boundary is too irregular, thus the fitting method does not give repeatable results, but any suitable threshold value is not discovered yet. - It fails for the laminar flow.
Flatness	- Refers to rare events at the wake boundary, thus it is the most physical method to find the wake edge. - The wake is drawn quite sharply.	- Need for high statistical quality. - It is not yet explored, how it behaves, when the background flow is turbulent. - It fails for the laminar flow.

To give some final recommendations, the wake width based on average velocity profile would be excellent for comparative studies, to determine, which variant of some construction element creates smaller wake. When the research goal points to mixing problems, to mechanical stability of other construction elements near the wake, to transportation safety issues or to the interaction of multiple wakes, then the higher statistical momenta have to be taken into account, but the skewness seems to behave too irregularly, therefore the flatness remains.

6.1. Future work

The present data have been measured past a prismatic airfoil inside a wind tunnel with minimal turbulence intensity. A natural question is, how the discussed wake widths would behave in the case of moderate or even high turbulence intensities, especially the skewness and flatness can be very sensitive to this issue and it can make impossible to find some threshold or peak in their profiles. At this moment, we do not know, this has to be explored by future experiments.

The natural continuation of this discussion leads to the measurement of fully three-dimensional wake past a more complex obstacle, than is the prismatic body used in the present study. Such wakes are usually measured in planes perpendicular to the incoming flow direction [Schottler2018]. In such planes, only the threshold method seems to make sense. The wake width will be renamed as wake area. This area is expected to be bounded by a closed curve, which is expected to converge to a circle in far wake or to the obstacle

contour in the near wake [Schottler2018]. But these speculations have to be confirmed or rejected by real experiment planed to the future.

We thank You for reading and look forward for the next experiments!

Supplementary Materials: The following are available online at www.mdpi.com/xxx/s1, Figure S1: title, Table S1: title, Video S1: title.

Author Contributions: Conceptualization, D.D. and V.Y.; methodology, V.U.; software, D.D.; validation, D.D; formal analysis, V.U.; investigation, D.D.; resources, D.D.; data curation, D.D.; writing—original draft preparation, D.D.; writing—review and editing, V.U and V.Y.; visualization, D.D.; supervision, V.U. All authors have read and agreed to the published version of the manuscript.

Funding: The scanning was supported from ERDF under project Research Cooperation for Higher Efficiency and Reliability of Blade Machines (LoStr) No. CZ.02.1.01/0.0/0.0/16_026/0008389. The APC has been paid by European Union, as part of the project entitled Development of capacities and environment for boosting the international, intersectoral and interdisciplinary cooperation at UWB, project reg. No. CZ.02.2.69/0.0/0.0/18_054/0014627.

Data Availability Statement: In this section, please provide details regarding where data supporting reported results can be found, including links to publicly archived datasets analyzed or generated during the study. Please refer to suggested Data Availability Statements in section "MDPI Research Data Policies" at https://www.mdpi.com/ethics. You might choose to exclude this statement if the study did not report any data.

Acknowledgments: We thank Buhumil Laštovka and Volodymyr Tsymbalyuk for technical help. We thank Petr Eret and Radka Lanči for help with the LoStr project. We thank Roman Čermák, Tetjana Tomášková and Lucie Komrsková for help with the Cooperation project.

Conflicts of Interest: The authors declare no conflict of interest.

References

1. Author 1, A.B.; Author 2, C.D. Title of the article. *Abbreviated Journal Name* **Year**, *Volume*, page range.
1. [Williamson1996] Williamson, C. H. K., Vortex Dynamics in the Cylinder Wake, *Annu Rev Fluid Mech* **1996** *28(1)*, 477-539, doi: 10.1146/annurev.fl.28.010196.002401
2. [Wu2019] Wu, X., Hu, W., Huang, Q., Chen, C., Chen, Z. and Blaabjerg, F. Optimized Placement of Onshore Wind Farms Considering Topography, *Energies* **2019**, *12(15)*, 2944, doi: 10.3390/en12152944
3. [Abdulrahman2019] Abdulrahman, M., Wood, D. Wind Farm Layout Upgrade Optimization, *Energies* **2019**, *12(13)*, 2465, doi: 10.3390/en12132465
4. [Karman1911] von Kármán, Th. Über den Mechanismus den Widerstands, den ein bewegter Korper in einer Flussigkeit erfahrt, *Göttinger Nachrichten, Math. Phys* **1911** Kl. 509 – 517
5. [Strouhal1878] Strouhal, V. Über eine besondere Art der Tonerregung, *Ann. Phys* **1878** *241* 216–251, doi: 10.1002/andp.18782411005
6. [Williamson1987] Williamson, C. H. K. Three-dimensional transition in the near wake of a cylinder, *Bull. American Phys. Soc.* **1987** *32*, 2098
7. [Williamson2006] Williamson, C. H. K., Three-dimensional wake transition *J Fluid Mech* **2006,** *328*, 345-407, doi: 10.1017/S0022112096008750
8. [Roshko1955] Roshko, A. On the wake and drag of bluff bodies, *J. Aeronaut. Sci* **1955,** *22*, 124, doi: 10.2514/8.3286
9. [Roshko1961] Roshko, A. Experiments on the flow past a circular cylinder at very high Reynolds number, *J. Fluid Mech.* **1961**, *10*, 345 – 356, doi: 10.1017/S0022112061000950
10. [Roshko1967] Roshko, A. Trsansition in incompressible near-wakes, *Phys. Fluids* **1967**, *10*(9), S181-S183, doi: 10.1063/1.1762441
11. [Sadeghi] Sadeghi, H. and Mani, M. The unsteady turbulent wake measurements behind an oscillating airfoil, *Turbul Heat Mass Transf* **2009**, *6*, 9, doi: 10.1615/ICHMT.2009.TurbulHeatMassTransf.2500
12. [Davary] Davary, A. Wake structure and similar behavior of wake profiles downstream of a plunging airfoil, Chinese J Aeronaut **2017**, *30*, doi: 10.1016/j.cja.2017.05.007
13. [Liu] Liu, X., Jawahar, K. H., Azarpeyvand, M and Theunissen, R. Wake Development of Airfoils with Serrated Trailing Edges, *AIAA* **2016**, 2817, doi: 10.2514/6.2016-2817
14. [Terra2016] Terra, W., Sciacchitano, A., Scarano, F. Drag analysis from PIV data in speed sports, *Procedia Engineer* **2016**, *147*, 50 – 55, doi: 10.1016/j.proeng.2016.06.188

15. [Hah] Hah, C. and Lakshminarayana, B. Measurement and prediction of mean velocity and turbulence structure in the near wake of an airfoil, *J Fluid Mech* **1982**, *115*, 251 – 282, doi: 10.1017/S0022112082000743
16. [Kunze] Kunze, C. Acoustic and Velocity Measurements in the Flow Past an Airfoil Trailing Edge, *Thesis University of Notre Dame* **2004**, url: https://curate.nd.edu/show/02870v85085
17. [Solis], Solís-Gallego, I. and Meana-Fernandez, A. and Oro, J. and Díaz, K.M.A. and Velarde-Suarez, S. Turbulence Structure around an Asymmetric High-Lift Airfoil for Different Incidence Angles, *J Appl Fluid Mech*, **2017**, *10*, 1013 – 1027, doi: 10.18869/acadpub.jafm.73.241.27625
18. [Tropea] Tropea, C., Yarin, A., Foss, J.F. Springer Handbook of Experimental Fluid Mechanics. *Springer, Heidelberg* **2006**, DE.
19. [Kopecký] Kopecký, V. Laserová anemometrie v mechanice tekutin, *Tribun, Liberec* **2008**, ISBN: 978-80-7399-357-3
20. [Inkinen2011] Inkinen, S., Hakkarainen, M., Albertsson, A.., Södergøard, A. From lactic acid to poly(lactic acid) (pla): Characterization and analysis of pla and its precursors. *Biomacromolecules* **2011**, *12*, 523–532, doi:10.1021/bm101302t.
21. [Duda2021b] Duda, D. How Manufacturing Inaccuracies Affect Vortices in an Airfoil Wake, *Proceedings of Topical Problems of Fluid Mechanics* **2021**, 48-55, doi: 10.14311/TPFM.2021.007
22. [Bém2019] Bém, J., Duda, D., Kovařík, J., Yanovych, V. and Uruba, V. Visualization of Secondary Flow in a Corner of a Channel, *AIP Conf Proc* **2019** *2189*, 020003, doi: 10.1063/1.5138615
23. [Duda2020] Duda, D., Bém, J., Yanovych, V., Pavlíček, P. and Uruba, V. Secondary flow of second kind in a short channel observed by PIV, *Eur J Mech B-Fluid* **2020**, *79*, 444-453, doi: 10.1016/j.euromechflu.2019.10.005
24. [Terra2017] Terra, W., Sciacchitano, A., Scarano, F. Aerodynamic drag of a transiting sphere by large-scale tomographic-PIV, *Exp Fluids* **2017**, *58*, 83, doi: 10.1007/s00348-017-2331-0
25. [Ragni2011] Ragni, D., van Oudheusden, B. W., Scarano, F. Non-intrusive aerodynamic loads analysis of an aircraft propeller blade, *Exp Fluids* **2011**, *51*, 361–371, doi: 10.1007/s00348-011-1057-7
26. [Gunasekaran2021] Gunasekaran, S. and Altman, A. Far Wake and Its Relation to Aerodynamic Efficiency, *Energies* **2021**, *14(12)*, 3641, doi: 10.3390/en14123641
27. [Barthelmie2006] Barthelmie, R. J., Frandsen, S. T., Rethore, P. E., Mechali, M., Pryor, S. C., Jensen, L., Sørensen, P. Modelling and measurements of offshore wakes, *Conference OWEMES* **2006**, 45 – 53, url: https://www.researchgate.net/publication/241698692
28. [Frisch] Frisch, U., Turbulence: The legacy of A. N. Kolmogorov, *Cambridge University Press*, **1995**, ISBN: 0 521 45713 0.
29. [Blondel2020] Blondel, F., Cathelain, M., Joulin, P. A., Bozonnet, P. An adaptation of the super-Gaussian wake model for yawed wind turbines, *J. Phys.: Conf. Ser.* **2020** *1618*, 062031, doi: 10.1088/1742-6596/1618/6/062031
30. [Eames2011] Eames, I., Jonsson, C., Johnson, P. B., The growth of a cylinder wake in turbulent flow, *J Turbul* **2011** *12*, N39, doi: 10.1080/14685248.2011.619985
31. [Norberg1986] Norberg, C., INTERACTION BETWEEN FREESTREAM TURBULENCE AND VORTEX SHEDDING FOR A SINGLE TUBE IN CROSS-FLOW, *J Wind Eng Ind Aerod* **1986**, *23*, 501—514, doi: 10.1016/0167-6105(86)90066-8
32. [Cao2018] Cao, Yo., Tamura, T. Aerodynamic characteristics of a rounded-corner square cylinder in shear flow at subcritical and supercritical Reynolds numbers, *J Fluid Struct* **2018**, *82*, 473-491, doi: 10.1016/j.jfluidstructs.2018.07.012
33. [Skrbek2021] Skrbek, L., Schmoranzer, D., Midlik, Š., Sreenivasan, K. R. Phenomenology of quantum turbulence in superfluid helium, *PNAS* **2021** *118*, 16, doi: 10.1073/pnas.2018406118
34. [LaMantia2013] La Mantia, M., Duda, D., Rotter, M., Skrbek, L. Lagrangian velocity distributions in thermal counterflow of superfluid 4He, *EPJ Web of Conferences* **2013** *45*, 01005, doi: 10.1051/epjconf/20134501005
35. [LaMantia2016] La Mantia, M., Švančara, P., Duda, D., Skrbek, L. Small-scale universality of particle dynamics in quantum turbulence, *Phys. Rev. B* **2016,** 94, 18, doi: 10.1103/PhysRevB.94.184512
36. [Duda2017] Duda, D., La Mantia, M. and Skrbek, L. Streaming flow due to a quartz tuning fork oscillating in normal and superfluid He 4, *Physical Review B* **2017** *96* (2) 024519, doi: 10.1103/PhysRevB.96.024519
37. [Mariotti2013], Mariotti, A., Buresti, G. Experimental investigation on the influence of boundary layer thickness on the base pressure and near-wake flow features of an axisymmetric blunt-based body, *Exp Fluids* **2013** *54*, 1612, doi: 10.1007/s00348-013-1612-5
38. [Sciacchitano2019] Sciacchitano, A. Uncertainty quantification in particle image velocimetry, Meas. Sci. Technol. **2019** *30*, 092001, doi: 10.1088/1361-6501/ab1db8
39. [Sciacchitano2016] Sciacchitano, A, Wieneke, B. PIV Uncertainty propagation, Meas. Sci. Technol. **2016** *27*, 084006, doi: 10.1088/0957-0233/27/8/084006
40. [Du2016] Du, W., Zhao, Yo., He, Ya., Liu, Ya. Design, analysis and test of a model turbine blade for a wave basin test of floating wind turbines, *Renew Ener* **2016** 97, 414 – 421, doi: 10.1016/j.renene.2016.06.008
41. [Schottler2018] Schottler, J. Bartl, J., Mühle, F., Sætran, L., Peinke, J., Hölling, M. Wind tunnel experiments on wind turbine wakes in yaw: redefining the wake width, *Wind Energ. Sci.* **2018**, *3(1)*, 257 – 273, doi: 10.5194/wes-3-257-2018